scientific reports

Check for updates

OPEN

Element-specific visualization of dynamic magnetic coupling in a Co/Py bilayer microstructure

Thomas Feggeler[1,6]✉, Ralf Meckenstock[1], Detlef Spoddig[1], Christian Schöppner[1], Benjamin Zingsem[1,2], Taddäus Schaffers[3], Hendrik Ohldag[4,5,6,7], Heiko Wende[1], Michael Farle[1], Andreas Ney[3] & Katharina Ollefs[1]

We present the element-specific and time resolved visualization of uniform ferromagnetic resonance excitations of a Permalloy (Py) disk–Cobalt (Co) stripe bilayer microstructure. The transverse high frequency component of the resonantly excited magnetization is sampled in the ps regime by a combination of ferromagnetic resonance (FMR) and scanning transmission X-ray microscopy (STXM-FMR) recording snapshots of the local magnetization precession of Py and Co with nanometer spatial resolution. The approach allows us to individually image the resonant dynamic response of each element, and we find that angular momentum is transferred from the Py disk to the Co stripe and vice versa at their respective resonances. The integral (cavity) FMR spectrum of our sample shows an unexpected additional third resonance. This resonance is observed in the STXM-FMR experiments as well. Our microscopic findings suggest that it is governed by magnetic exchange between Py and Co, showing for the Co stripe a difference in relative phase of the magnetization due to stray field influence.

For future information technology new concepts are needed involving the charge of the electron as well as its spin as information unit[1]. Several approaches for magnetism based logic have been introduced, ranging from soliton based concepts[2], to magnonics in the form of e.g. genetically engineered magnonic computing[3,4] to overcome the various limitations, e.g. thermal load and energy needs, encountered by modern computer technology. This field of spintronics and magnonics requires to study even smaller magnetic structures in the gigahertz and terahertz regime.

Spin-based devices usually consist of more than one material, requiring the understanding of the element-specific dynamic magnetic properties and the resulting spin wave modes on the nanometer scale. X-ray detected ferromagnetic resonance (XFMR)[5–13], combining ferromagnetic resonance (FMR) with element specific magnetometry by means of X-ray Magnetic Circular Dichroism (XMCD) (see[14,15] and references therein) is a unique tool to address this challenge.

In this study Scanning Transmission X-ray Microscopy detected FMR (STXM-FMR)[16] has been used, offering temporal sampling down to 17 ps and nominal sub 50 nm lateral resolution in transverse XFMR geometry with a continuous wave excitation of the sample[16–21]. Uniform and non uniform resonant responses on the micro-[22,23] and sub 50 nm nanometer[24] scale have been monitored and analysed. Here we investigate resonant excitations of a bilayered microstructure consisting of a Cobalt (Co) stripe deposited on a Permalloy (Py) disk with element specificity. Earlier studies of equally dimensioned ultra-thin ferromagnetic bilayers (thickness usually about or below 10 nm) showed two uniform resonance modes, typically explained as an in-phase and out-of-phase optical or acoustical modes e.g.[25]. In the conventional FMR measurements of our bilayer microstructure with a total thickness of 60 nm the individual resonances of the Py and Co microstructures are identified. In addition, a third resonance in both materials is seen, which cannot be explained by the aforementioned approach for equally dimensioned ultra-thin bilayers, but by Py and Co resonating in phase as an entity, mediated by exchange

[1]Faculty of Physics and Center for Nanointegration Duisburg-Essen (CENIDE), University of Duisburg-Essen, 47048 Duisburg, Germany. [2]Ernst Ruska Centre for Microscopy and Spectroscopy with Electrons and Peter Grünberg Institute, Forschungszentrum Jülich GmbH, 52425 Jülich, Germany. [3]Institute of Semiconductor and Solid State Physics, Johannes Kepler University Linz, 4040 Linz, Austria. [4]SLAC National Accelerator Laboratory, Menlo Park, CA 94025, USA. [5]Department of Physics, University of California Santa Cruz, Santa Cruz, CA 95064, USA. [6]Present address: Advanced Light Source, Lawrence Berkeley National Laboratory, Berkeley, CA, USA. [7]Department of Material Sciences and Engineering, Stanford University, Stanford, CA 94305, USA. ✉email: tfeggeler@lbl.gov

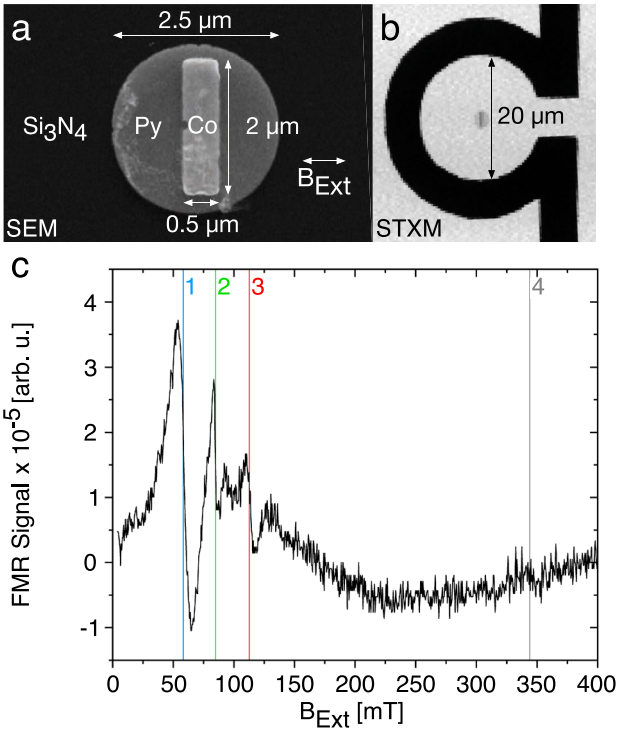

Figure 1. (**a**) Scanning electron microscopy (SEM) image of the Co stripe/Py disk bilayer on a Si_3N_4 membrane. The orientation of B_{ext} is indicated; (**b**) STXM image of the sample in the micro-resonator loop; The high-frequency magnetic field oscillates in the out-of-plane direction (**c**) FMR spectrum of the sample shown in a) with four major resonances, 1: Py resonance, 2: Coupled resonance, 3: Co stripe center resonance, 4: Resonance of the long sides of the Co stripe.

coupling. Thus, by our spatially, time and element specific STXM-FMR the origin of the three resonances is revealed, visualizing as well local phase and amplitude variations, which are not visible in conventional FMR spectra.

Methods

We measure FMR excitations in their linear regime using a micro-resonator based, element-specific and spatially resolved STXM-FMR setup realized at Stanford Synchrotron Radiation Lightsource (SSRL)[16,18]. The sample is a polycrystalline Co stripe (2.0 µm length, 0.5 µm width, 30 nm thickness) deposited on a polycrystalline Permalloy(Py)-disk with 2.5 µm diameter and 30 nm thickness (see Fig. 1a). It is fabricated by a three step lithography and electron-beam deposition of the ferromagnetic material[26] on a 200 nm thick Si_3N_4 membrane. To measure the FMR spectrum the sample is positioned in the omega-shaped loop of a micro-resonator offering a sensitivity of 10^6 μ_B[27–29]. The sample is excited by a homogeneous linearly polarized microwave field with an amplitude of ≤ 1.5 mT. A STXM image of the sample using a step size of 100 nm is shown in Fig. 1b.

Figure 1c pictures the conventional FMR spectrum of the sample obtained at a microwave frequency of 9.27 GHz in a magnetic field $B_{Ext} = 0$–200 mT featuring three main resonances, the first resonance at $B_{Ext,1} = 58.3$ mT, the second resonance at $B_{Ext,2} = 84.9$ mT, and the third resonance at $B_{Ext,3} = 112.7$ mT. An additional fourth resonance we identify at $B_{Ext,4} = 344$ mT with a line width of about 8 mT corresponding to an edge mode of the Co stripe, as shown e.g. in[28,29]. In our STXM-FMR setup only the three resonances below 200 mT can be recorded due to the limit of the available B_{Ext}. Resonances 1 and 3 are modes of the Py disk and the Co stripe, respectively. Magneto-crystalline anisotropy is neglible in both samples due to their polycrystallinity. The Co stripe exhibits the highest resonance field due to shape anisotropy despite its high $M_{sat} = 1420$ kA/m [30] considering the stripe geometry and the perpendicular orientation of its long side to B_{Ext} (Fig. 1a), while Py with $M_{sat} = 860$ kA/m[30] shows the lowest resonance field. This is confirmed by angular dependent FMR measurements of a Co stripe[29]. The origin of the intermediate resonance 2, however, can not readily be understood, because one would only expect the two individual resonances. The presence of a third resonance at an intermediate field strongly suggests that Co and Py resonate as one entity resulting in a coupled uniform resonance. Although it appears reasonable to assume that this is due to exchange coupling across the interface, it is not possible to directly deduce the microscopic mechanism behind our observation from the classical FMR spectrum. To elucidate this, we use STXM-FMR.

In STXM-FMR the sample is mapped by a focussed X-ray beam (energy tunable between 200 eV and 1200 eV at the SSRL), while the transmitted intensity is detected by an avalanche X-ray photodiode. B_{ext} is applied in the sample plane along the short axis of the Co stripe (Fig. 1a)) with perpendicular orientation to the incident

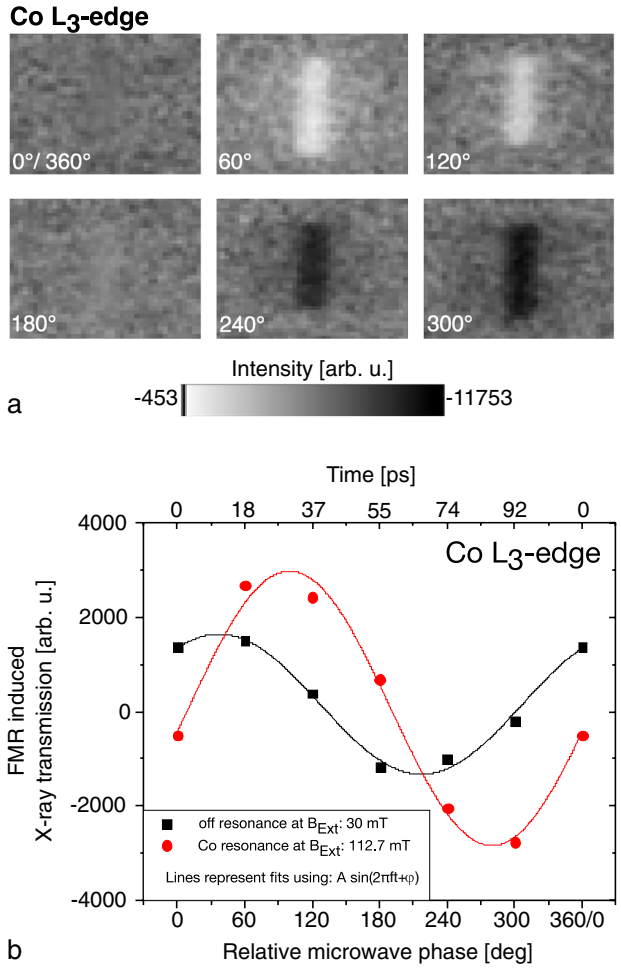

Figure 2. (**a**) 6 STXM-FMR difference images obtained from six microwave on and six microwave off images recorded every 60° (18 ps) at the Co L_3-edge at $B_{Ext,3}$. (**b**) FMR induced X-ray transmission signal (red dots: at Co resonance 3, black squares: off resonance) as function of time.

circularly polarized X-rays. The time-dependent transverse component of the magnetization at 9.129 GHz is probed by means of the XMCD effect, for details see[16]. The magnetization oscillation is sampled with 6 consecutive images separated by a static phase difference of 60° (18 ps), each with and without applied microwave excitation. To extract the microwave induced X-ray absorption the respective difference of both datasets is taken. Fig. 2a) shows the resulting 6 STXM-FMR images at the Co L_3-edge with an applied external magnetic field of 112.7 mT (Fig. 1b). Brighter and darker contrast indicates a lower/higher X-ray absorption than the average. The contrast within the area of the Co stripe indicates a microwave induced response. Thus, the bright and dark contrast in Fig. 2a) shows the deviations of the magnetization from its equilibrium orientation along the oscillation axis of the high frequency magnetic field. Figure 2b shows the oscillation of the STXM-FMR signal at the position of the Co stripe. Its maximum is visible at a relative phase of about 90°. The black curve in Fig. 2b was recorded at an off resonance field of 30 mT and thus the Co is only driven by the microwave field. The red STXM-FMR signal is shifted by 90°, as generally expected for a resonant response[31].

Results and discussion

The element-specific and spatially resolved measurements depicted in Fig. 3 show the STXM-FMR images at the Ni L_3-edge (852 eV) (Fig. 3a–c), and Co L_3-edge (779 eV) (Fig. 3d–f) taken at a relative phase of 300° exhibiting the highest contrast, with a 100 nm step size and a dwell time of 5000 ms. Grey contrast corresponds to an average contrast value, which is set to the same background color level for all images of the figure. In Fig. 3a–c the complete circular area of the Py disk shows STXM-FMR contrast at all three resonance fields, indicating a resonant response of the Py disk. Each of STXM-FMR images in Fig. 3a–c) reveals a darker colored contrast area at the location of the on-top lying Co stripe. Fig. 3d–f picture the STXM-FMR contrast originating from Co stripe while the Py disk is almost invisible with the The STXM-FMR image at resonance 3 (Fig. 3f) showing the darkest coloured contrast of all the images (Fig. 3d–f).

The STXM-FMR image taken at resonance 1 shown in Fig. 3a (Ni L_3-edge) shows a uniform contrast distribution within the disk area with a higher intensity contrast area at the position of the Co stripe. This is

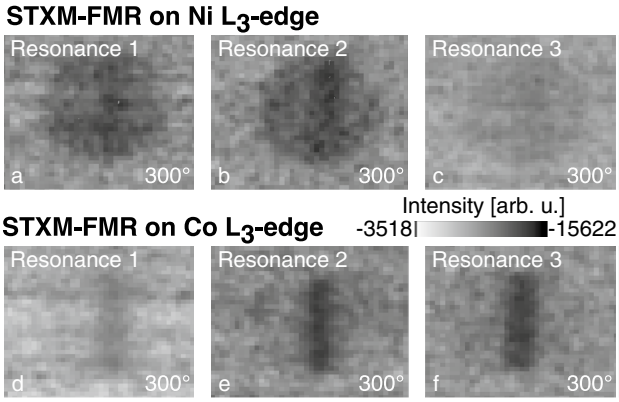

Figure 3. STXM-FMR images taken at the respective B_{ext} for resonance 1, 2, and 3. (**a**)–(**c**) are recorded at the Ni L_3-edge, (**d**, **e**) are recorded at the Co L_3-edge. The STXM-FMR images correspond to the time slot at 92 ps (300°).

corresponding to a homogeneous uniform resonant response of the Py disk as expected from the conventional FMR spectrum (Fig. 1a). The contrast visible in Fig. 3d within the Co stripe originates from Co being driven by the Py in resonance, inducing a slight increased precessional motion in the Py disk (higher intensity contrast area in Fig. 3a) mediated by exchange coupling. The corresponding observation is made for the Py disk at $B_{ext,3}$, where the Py magnetic moments are less agile due to their alignment along the direction of B_{ext}, resulting in the Py disk getting only slightly driven by the Co in resonance. In consequence the contrast of the driven Co in Fig. 3d is more intense than the one of the driven Py in Fig. 3c as the Co moments are not completely aligned along $B_{ext,1}$ and therefore are more agile and easily driven compared to the Py moments of the disk at $B_{ext,3}$. This excitation between the two constituents across the interface illustrates a transfer of angular momentum (spin current) between the two magnetic materials due to exchange coupling.

At resonance 2 the STXM-FMR images at both absorption edges show uniformly distributed contrast at the location of both of the sample constituents, indicating a coupled resonance originating from exchange coupling between Py and Co both being in resonance and contributing to the STXM-FMR signal. Such modes have been observed before in multilayer films and originate in the interface exchange between both constituents. The exchange length in Co and Py is several nanometers, thus in ferromagnetic resonance the sample behaves in this area alloy-like. This can be seen for example in[32], where spin wave spectra exist at an effective magnetization of FeNi as an alloy-like entity in addition to the individual spin-wave resonance of Fe. Our STXM-FMR measurements of resonance 2 show at the Ni L_3 edge that the resonance can be observed in the whole area of the disc with a darker contrast at the position of the Co stripe/interface, broader than the contrast seen at the Co L_3edge, since the edge spins of Co are still not aligned along $B_{ext,2}$ and thus not in resonance. This is due to that beside the exchange length for this excitation the coherence length of the FMR precession is important, which ranges depending on the material up to several millimeters (e.g. tens of μm for Py[33]). In consequence the intensities of the three resonance modes shown in Fig. 2b consistent to this interpretation. The Py resonance 1 shows the highest intensity due to the largest sample volume, therefore the coupling resonance 2 shows less intensity as it originates as described above only from a part of the sample, while the Co resonance 3 exhibits the lowest intensity, corresponding to the smallest excited volume.

The magnetization orientation and the influence of magnetic dipolar coupling at resonance 2 has been visualized by micromagnetic simulations using MuMax3[34,35]. A Py disk (2500 nm×30 nm)/Co stripe (2000 nm× 500 nm×30 nm) bilayer microstructure is simulated at B_{Ext} = 85 mT, orientated as pictured in Fig. 1a. The simulation parameters are 860 kA/m (Py) and 1420 kA/m (Co) as saturation magnetization (both values[30]) and 13×10^{-12} J/m (Py) and 30×10^{-12} J/m (Co) as exchange stiffness (both values[36]). The simulation grid consists of 502 × 502 × 14 cells with equally dimensioned cells of 5 × 5 × 5 nm^3, lying below the exchange length of 5.3 nm (Py, e.g.[37]) and 8.1 nm (Co, e.g.[38]). The two-dimensional magnetization distribution after relaxation under field from a random initial state is shown in Fig. 4a,b for both sample constituents. The different orientation of the magnetization towards the long stripe edges can be clearly seen in the Co stripe, as well as imprinted to the Py disk. The demagnetization/stray field intensity is pictured in Fig. 4c,d for the Py disk and the Co stripe respectively. Fig. 4c clearly indicates the influence of the Co stripe on the Py disk due to magnetic dipolar interaction due to the higher value of the demagnetization field intensity of about 100 mT at the position of the stripe. It becomes apparent from Fig. 4 that the magnetization in the Co stripe is not saturated at B_{Ext} = 85 mT, with the Co magnetic moments not aligned along the field direction at the long stripe edges, as indicated in Fig. 4b. This differently orientated magnetization towards the Co Stripe edges effectively results in a different resonance field of the edges, which manifests itself by the presence of the edge-resonance at B_{Ext} = 344 mT (resonance 4) shown in Fig. 1c.

An amplitude and phase analysis of the recorded 6 STXM-FMR images[39] at resonance 2, shown in Fig. 4c,d at the Ni and Co L_3-edge, reveals further details on the origin of the FMR excitations, not directly visible in the grayscale plots. After normalising the STXM-FMR data to the average intensity of each image, a sine fit is applied

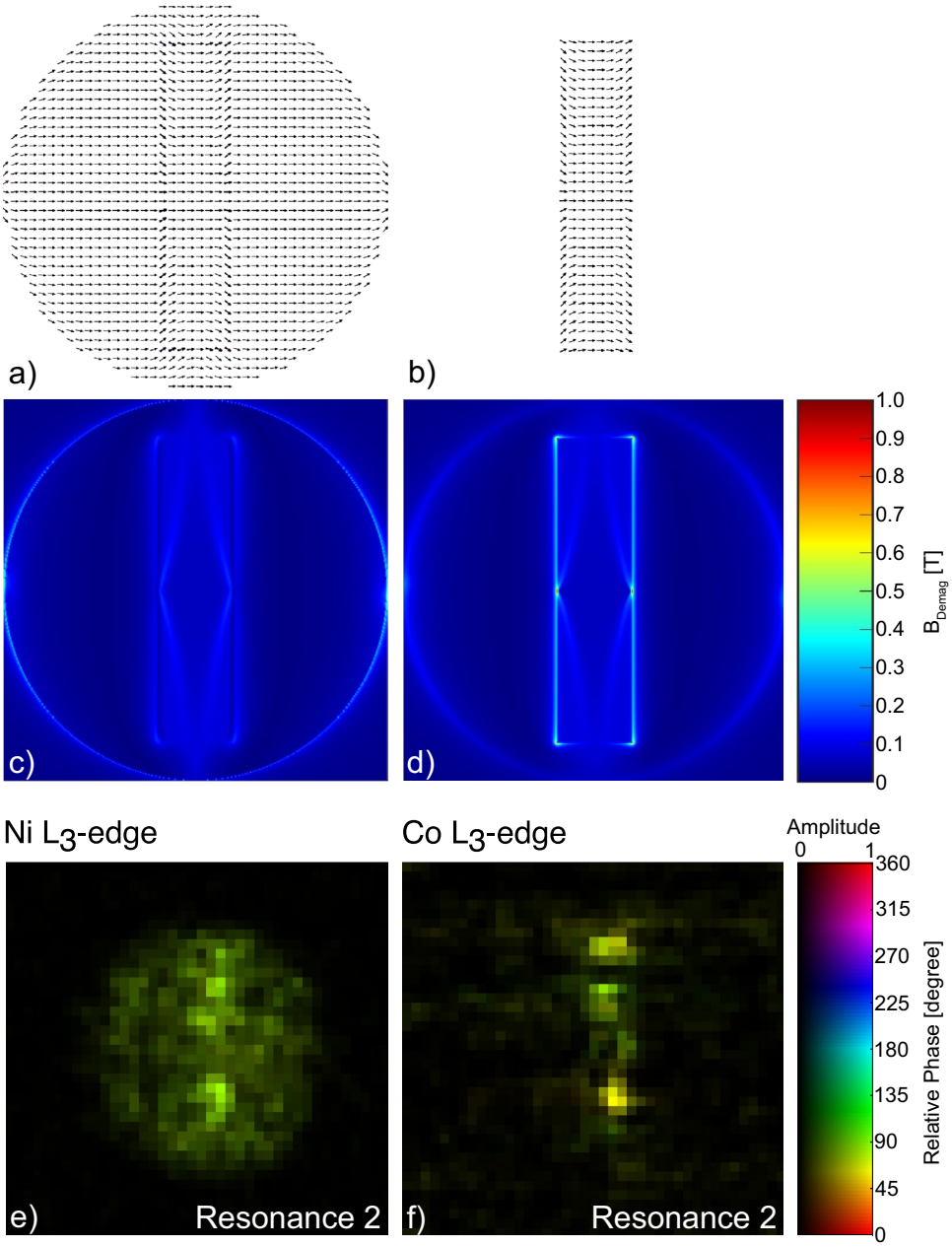

Figure 4. (**a**, **b**) Simulated two-dimensional representation of the magnetization distribution for the Py disk and the Co stripe, respectively. (**c**, **d**) picture the corresponding demagnetization- and stray field intensities, representing the center layer of the simulated geometry. (**a**–**d**) were simulated at B_{Ext} = 85 mT orientated perpendicular to the long sides of the Co stripe. (**e**, **f**) Result of the pixel-wise fit analysis of the STXM-FMR images, the color coding of the amplitude and relative phase is displayed by the color bar. The STXM-FMR images represent resonance 2 visible at 84.9 mT in Fig. 1c.

to the time evolution of each pixel. Thus, the pixels of the STXM-FMR image can be color coded representing amplitude, phase and fit accuracy obtained from the sinusoidal fits. The color coding was chosen as such that bright pixels represent a large amplitude, the phase is represented as the hue value and pixels with very high saturation indicate a high fit accuracy by encoding the p-value obtained from the fit as color saturation. Thus, Fig. 4e indicates a homogeneously distributed relative phase of approximately 90° to the exciting microwave inside the whole Py disk, whereas the amplitude of the Py excitation is largest at the position of the upper and lower edge of the Co stripe, which is not directly visible in Fig. 3b. Figure 4f shows bright and saturated colored pixels only at the position of the Co stripe, depicting different phase values between the center (approx. 90° as with the Py) and the upper and lower edges (poles) of the Co stripe (approx. 60°), due to, as for a typical bar magnet, the stray field influence. This leads to a different phase at the top and bottom edges of the Co stripe. The local phase change is only resolvable with our technique. Figure 4e,f prove that the exchange coupled resonance 2 is

mainly excited at the directly overlapping areas of disk and stripe and is not due to either an optical or acoustical mode excitation, both Py and Co are resonating at the field value corresponding to the one of an alloy-like entity, which is proven by similar phases.

The STXM-FMR observation of the three resonances is in agreement with the line widths observed in Fig. 1c. The largest peak to peak line width of 15 mT is observed at resonance 1, where the whole Py disk is in resonance but drives the Co moments at the area of the Co stripe. This yields an additional damping for the Py and an additional line distribution resulting from the area outside and below the stripe. The same is valid for the Co resonance 3 (peak to peak line width of 10 mT), there the Co is driving the Py underneath, which is already completely aligned with the external field and thus provides a stronger damping. The coupling resonance 2 has the smallest peak to peak line width (about 5 mT). In addition, an asymmetric line shape of the resonance is visible indicating a distribution of different excitations.

Conclusion

The magnetization dynamics of a coupled Py disk Co stripe bilayer microstructure has been analyzed in the linear response regime with element specificity, spatial, time and phase resolution. At the Py resonance the Co magnetization is driven into precession by angular momentum transfer mediated by exchange coupling of the precessing Py. We show in our experiment that a coherently precessing spin polarization is transferred via intermaterial exchange at the interface to the ferromagnetic material, which is not in resonance.

In earlier investigations of extended ferromagnetic ultra-thin bilayers two main resonances have been observed attributed to an in-phase and out-of-phase optical or acoustical mode[25]. In contrast here we revealed in the bilayered microstructure the occurrence of a third main resonance mode, which is explained by Py and Co resonating as an exchanged coupled entity. Using an amplitude and phase analysis method an inhomogeneous excitation of the Co stripe at the coupled resonance is revealed, due to the stray field effects at the poles of the stripe, whose influence is visualized by micromagnetic simulations. Thus, this mode is identified as an exchange coupled and dipolarly influenced excitation of the Co/Py disk stripe microstructure.

Data availability

The datasets used and/or analyzed during the current study are available from the corresponding author on reasonable request.

Received: 16 May 2022; Accepted: 27 October 2022
Published online: 04 November 2022

References

1. Wolf, S. A. *et al.* A spin-based electronics vision for the future. *Science* **294**, 1488 (2001).
2. Cowburn, R. P. & Welland, M. E. Room temperature magnetic quantum cellular automata. *Science* **287**, 1466 (2000).
3. Zingsem, B. W. *et al.* Biologically encoded magnonics. *Nat. Commun.* **85**, 4345 (2019).
4. Barman, A. *et al.* The 2021 magnonics roadmap. *J. Phys. Condens. Matter* **33**, (2021).
5. Bailey, W. E. *et al.* Precessional dynamics of elemental moments in a ferromagnetic alloy. *Phys. Rev. B* **70**, (2004).
6. Marcham, M. K. *et al.* Phase-resolved X-ray ferromagnetic resonance measurements in fluorescence yield. *J. Appl. Phys.* **109**, 07D353 (2011).
7. Bailey, W. E. *et al.* Detection of microwave phase variation in nanometre-scale magnetic heterostructures. *Nat. Commun.* **4**, 2025 (2013).
8. Goulon, J. *et al.* X-ray detected magnetic resonance at the Fe K-edge in YIG: Forced precession of magnetically polarized orbital components. *JETP Lett.* **82**, 11 (2005).
9. Boero, G. *et al.* X-ray ferromagnetic resonance spectroscopy. *Appl. Phys. Lett.* **87**, (2005).
10. Goulon, J. *et al.* X-ray detected magnetic resonance of YIG thin films in the nonlinear regime of spin waves. *J. Magn. Magn. Mater.* **322**, 2308 (2010).
11. Boero, G. *et al.* Longitudinal detection of ferromagnetic resonance using X-ray transmission measurements. *Rev. Sci. Instrum.* **80**, (2009).
12. Boero, G. *et al.* Double-resonant X-ray and microwave absorption: Atomic spectroscopy of precessional orbital and spin dynamics. *Phys. Rev. B* **79**, (2009).
13. Ollefs, K. *et al.* Toward broad-band X-ray detected ferromagnetic resonance in longitudinal geometry. *J. Appl. Phys.* **117**, (2015).
14. Dürr, H. A. *et al.* A closer look into magnetism: Opportunities with synchrotron radiation. *IEEE Trans. Magn.* **45**, 15 (2009).
15. van der Laan, G. & Figueroa, A. I. X-ray magnetic circular dichroism—A versatile tool to study magnetism. *Coordin. Chem. Rev.* **95**, 277 (2014).
16. Bonetti, S. *et al.* Microwave soft X-ray microscopy for nanoscale magnetization dynamics in the 5–10 GHz frequency range. *Rev. Sci. Instr.* **86**, (2015).
17. Cheng, Ch. & Bailey, W. E. Sub-micron mapping of GHz magnetic susceptibility using scanning transmission X-ray microscopy. *Appl. Phys. Lett.* **101**, (2012).
18. Schaffers, T. *et al.* The combination of micro-resonators with spatially resolved ferromagnetic resonance. *Rev. Sci. Instrum.* **88**, (2017).
19. Groß, F. *et al.* Nanoscale detection of spin wave deflection angles in permalloy. *Appl. Phys. Lett.* **114**, 012406 (2019).
20. Sluka, V. *et al.* Emission and propagation of 1D and 2D spin waves with nanoscale wavelengths in anisotropic spin textures. *Nat. Nanotechnol.* **14**, 328 (2019).
21. Weigand, M. *et al.* A shot-noise limited, time-resolved pump-and-probe acquisition system capable of 50 GHz frequencies for synchrotron-based X-ray microscopy. *Crystals* **12**, 1029 (2022).
22. Pile, S. *et al.* Non-standing spin-waves in confined micrometer-sized ferromagnetic structures under uniform excitation. *Appl. Phys. Lett.* **116**, (2020).
23. Pile, S. *et al.* Direct imaging of the AC component of pumped spin polarization with element specificity. *Phys. Rev. Appl.* **14**, (2020).
24. Feggeler, T. *et al.* Spatially resolved GHz magnetization dynamics of a magnetite nano-particle chain inside a magnetotactic bacterium. *Phys. Rev. Res.* **3**, (2021).
25. Heinrich, B. *et al.* Structural and magnetic properties of ultrathin Ni/Fe bilayers grown epitaxiaiiy on Ag(001). *II Phys. Rev. B.* **38**(18), 12879 (1988).

26. Posth, O., Reckers, N., Meckenstock, R., Dumpich, G. & Lindner, J. J. Study of spin transfer torque in serially connected pillars by means of ferromagnetic resonance. *Phys. D. Appl. Phys.* **42**, (2009).
27. Banholzer, A. *et al.* Visualization of spin dynamics in single nanosized magnetic elements. *Nanotechnology* **22**, (2011).
28. Meckenstock, R. Invited Review Article: Microwave spectroscopy based on scanning thermal microscopy: Resolution in the nanometer range. *Rev. Sci. Instrum.* **79**, (2008).
29. Schöppner, C. *et al.* Angular dependent ferromagnetic resonance analysis in a single micron sized cobalt stripe. *J. Appl. Phys.* **116**, (2014).
30. Jiles, D. *Introduction to Magnetism and Magnetic Materials* 3rd edn. (CRC Press Taylor and Francis Group, 2016).
31. Pain, H. J. *The Physics of vibrations and waves* (Wiley, 2005).
32. Kordecki, R. *et al.* Spin wave resonance in FeNi multilayers. *J. Magn. Magn. Mater.* **93**, 281 (1991).
33. Kithun, A., Bao, M. & Wang, L. Spin wave magnetic NanoFabric: A new approach to spin-based logic circuitry. *IEEE Trans. Magn.* **44**, 2141–2152 (2008).
34. Vansteenkiste, A. *et al.* The design and verification of MuMax3. *AIP Adv.* **4**, (2014).
35. Exl, L. *et al.* LaBonte's method revisited: An effective steepest descent method for micromagnetic energy minimization. *J. Appl. Phys.* **115**, 17D118 (2014).
36. Donahue, M. J. & Porter, D. G. *OOMMF User's Guide, Version 1.0, Interagency Report NISTIR 6376* (National Institute of Standards and Technology, Gaithersburg, MD, 1999).
37. Wang, J. *et al.* Magnetic domain wall engineering in a nanoscale permalloy junction. *Appl. Phys. Lett.* **111**, (2017).
38. Bautin, V. A., Seferyan, A. G., Nesmeyanov, M. S. & Usov, N. A. Magnetic properties of polycrystalline cobalt nanoparticles. *AIP Adv.* **7**, (2017).
39. Zingsem, B., Feggeler, T., Meckenstock, R., Schaffers, T., Pile, S., Ohldag, H., Farle, M., Wende, H., Ney, A., Ollefs, K. (2019) arXiv: 1901.10595 [cond-mat.str-el].

Acknowledgements

The authors would like to thank the German Research Foundation (DFG projects: 321560838 (OL513/1-1) 405553726 TRR 270) and the Austrian Science Fund (FWF project: I 3050-N36) for financial support. We gratefully acknowledge the experimental assistance of S. Bonetti during beamline setup. The use of the Stanford Synchrotron Radiation Lightsource, SLAC National Accelerator Laboratory, is supported by the US Department of Energy, Office of Science, Office of Basic Energy Sciences under Contract No. DE-AC02-76SF00515.

Author contributions

R.M., D.S., K.O. and A.N. conceived the experiment(s), R.M., D.S., A.N., C.S. and H.O. conducted the experiment(s), T.F. performed the micromagnetic simulations, T.F., K.O., R.M. and D.S. analysed the data, T.F., K.O., R.M wrote the manuscript with support from D.S., B.Z., T.S., H.W., M.F. and H.O. All authors reviewed the manuscript.

Funding

Open Access funding enabled and organized by Projekt DEAL.

Additional information

Correspondence and requests for materials should be addressed to T.F.

Reprints and permissions information is available at www.nature.com/reprints.

Publisher's note Springer Nature remains neutral with regard to jurisdictional claims in published maps and institutional affiliations.

Open Access This article is licensed under a Creative Commons Attribution 4.0 International License, which permits use, sharing, adaptation, distribution and reproduction in any medium or format, as long as you give appropriate credit to the original author(s) and the source, provide a link to the Creative Commons licence, and indicate if changes were made. The images or other third party material in this article are included in the article's Creative Commons licence, unless indicated otherwise in a credit line to the material. If material is not included in the article's Creative Commons licence and your intended use is not permitted by statutory regulation or exceeds the permitted use, you will need to obtain permission directly from the copyright holder. To view a copy of this licence, visit http://creativecommons.org/licenses/by/4.0/.

© The Author(s) 2022